Inverse Kinematics of a Spatial Mechanism using Multibond Graph

Aman Kumar MAINI, Anand VAZ

Department of Mechanical Engineering
Dr. B. R. Ambedkar National Institute of Technology
Jalandhar – 144011, Punjab, India
e-mail: anandvaz@ieee.org
*Corresponding Author e-mail: amanmaini1975@gmail.com

Various methods are available to compute kinematics and dynamics in the case of spatial mechanisms. These methods are cumbersome and laborious for large and multibody spatial mechanisms. The bond graph technique is a powerful alternative tool for modeling. A four-link closed-chain 3R2S (3Revolute 2Spherical) spatial mechanism stands out among the other four-link closed-chain spatial mechanisms due to its ability to be used in a number of applications. The main aim of this paper is to compute the inverse kinematics of the mechanism using the bond graph structure of the system. In this paper, modeling of a four-link closed-chain 3R2S spatial mechanism has been conducted using a multibond graph approach. Inverse kinematics of the spatial mechanism, under various applications, has been directly obtained from the bond graph modeling. MATLAB coding for simulation has been done directly from the multibond graph without explicitly deriving system equations. The simulation results have been analyzed and discussed using various plots.

Keywords: bond graph, spatial mechanism, kinematics, modeling, simulation.

NOMENCLATURE

$_{j}^{k}\overline{r}_i$ – position of point i with respect to point j and expressed in frame k; $\in \mathbb{R}^3$,

$_{j}^{k}\dot{\overline{r}}_i$ – velocity of point i observed in frame j and expressed in frame k; $\in \mathbb{R}^3$,

$^{0}\overline{p}_C$ – translational momentum of a rigid body about its center of mass C, expressed in inertial frame 0; $\in \mathbb{R}^3$,

$_{C}^{0}I_B$ – inertia tensor of a rigid body B about its center of mass C, expressed in the inertial frame 0; $\in \mathbb{R}^{3\times3}$,

$_{0}^{0}\overline{\omega}_B$ – angular velocity of a rigid body B, observed and expressed in inertial frame 0; $\in \mathbb{R}^{3\times3}$,

$_{C}^{0}\overline{p}_B$ – angular momentum of a rigid body B about its center of mass C, expressed in inertial frame 0; $\in \mathbb{R}^{3\times3}$,

${}^0\overline{\tau}_j$ – torque applied on link j expressed in inertial frame 0; $\in \mathbb{R}^3$,
${}^0_k R$ – rotation matrix describing the orientation of frame k with respect to inertial frame 0; $\in \mathbb{R}^{3 \times 3}$,
${}^0\overline{F}_i$ – force acting on point i expressed in inertial frame 0; $\in \mathbb{R}^3$.

1. INTRODUCTION

A mechanism consists of a number of rigid links that are interconnected by various types of joints such as revolute, prismatic, cylindrical or spherical. The various solutions to achieve kinematics of such mechanisms have been explained in the literature [1–5].

For the dynamics of mechanisms, various formulations such as the Newton-Euler, Lagrange-Euler, and Hamilton method are found in several references [3, 4, 6]. Energy-based formulations such as the Euler-Lagrange method and Hamilton method, commonly used for modeling dynamics of physical systems, usually tend to be too mathematically inclined and cumbersome for large multi-body systems.

Bond graph, introduced by Henry Paynter in 1959, may also be used for modeling kinematics as well as dynamics of a system [7–12]. The bond graph methodology: a graphical representation of the dynamics of the system has been elaborately explained in several references, e.g. [11, 12]. The multibond graph has been applied for the modeling of rigid body systems since 1985 [8]. The bond graph technique has been used by many researchers [13–20] for modeling various mechanisms. The bond graph represents the transaction of power and causality between various elements of a system. The derivation of system equations from the bond graph is algorithmic and often derived by computer software, especially in the case of large systems.

One of the approaches to model the dynamics of mechanisms using bond graph is to start with the construction of the kinematic framework in graphical form based on linear and angular velocity relations. This is also referred to as the flow mapping approach in bond graphing. The translational and rotational inertias are suitably appended to this structure. The rigid links are graphically connected at joints using appropriate couplings, either translational or rotational. The graphical representation of causality using a bond graph can be employed to obtain the dynamics of the mechanism in various formulations, like the energy-based formulations of the Lagrange-Euler technique, Hamilton's method, etc. [21]. However, none of the available works in the literature suggest how the inverse kinematics may be obtained directly from the bond graph structure. The present work addresses this very issue and systematically demonstrates the methodology using the example of the 3R2S spatial mechanism. The utility of this commonly used mechanism is discussed in Sec. 3.

Since the different energy-based formulations can be derived from the bond graph model [21–25], it would be pointless to make a comparison of these methods.

One can also write a code for simulation algorithmically directly from the bond graph structure of a system, even without formal derivation of system equations.

In this paper, inverse kinematics of 3R2S spatial mechanism, under various applications, has been directly obtained from the bond graph structure. Simulation coding has been written directly from the bond graph of the system algorithmically. The various kinematic variables, such as joint angles, have been calculated and analyzed using various plots.

The paper is organized as follows: modeling of the mechanism is discussed in the next section. Section 3 describes various applications of the mechanism. Simulation results and discussion are explained in Sec. 4. Various applications of the mechanisms, along with plots of obtained trajectories and variations in joint angles, are mentioned in the same section. Section 5 presents the conclusion.

2. Modeling of a 3R2S spatial mechanism

The schematic diagram of a 3R2S spatial mechanism is shown in Fig. 1. The considered mechanism has four rigid links connected to each other using three revolute (3R) and two spherical (2S) joints. The reference frames are assigned at each joint using the Denavit-Hartenberg (DH) conventions [3]. Frame {0} is the
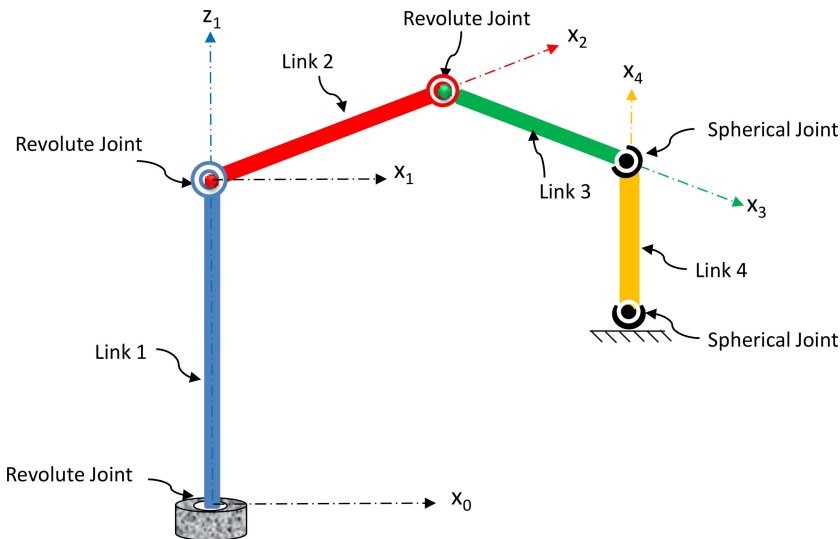
Fig. 1. 3R2S closed chain spatial mechanism.

inertial frame. In Fig. 2, link 1 is connected to the inertial frame by a revolute joint at point Q_1. Link 1 has rotary movement about its Z_1 axis. The second end P_1 of this link is connected to link 2 at point Q_2. Link 1 and link 2 are connected using a revolute joint. Similarly, second end P_2 of link 2 is connected to link 3 by a revolute joint at point Q_3. Link 3 is connected to link 4 at point P_3 by a spherical joint. The end point of link 4 is connected to a fixed frame by a spherical joint at point P_4. θ_1 is taken as the angle between the X_0-axis and X_1-axis. Similarly, θ_2 is the angle between link 1 and link 2. Angle θ_3 and angle θ_4 show the position of link 3 and link 4 in relation to link 2 and link 3, respectively.
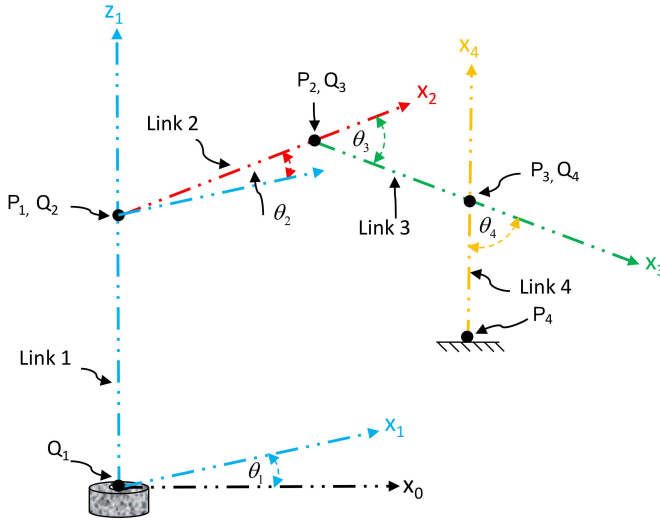
FIG. 2. Schematic diagram of the mechanism.

For modeling dynamics of the mechanism, each link of the mechanism has been considered as a separate rigid link. Modeling of a rigid link using a multi-bond graph approach has been explained in detail by Vaz [26] and Mishra and Vaz [27]. Here, a brief review of this procedure is presented considering one link of the mechanism. The flow mapping approach, based on the kinematics, is used to initiate the bond graph modeling of the system. For example, link 1 of the mechanism, shown in Fig. 3, is considered. The end points of this link are Q_1 and P_1, as shown in Fig. 3. The link has a revolute joint at point Q_1. Point Q_1 coincides with the origin O_1, which is at the origin 0 of the inertial frame.

Let $_0^0\bar{r}_{P_1}$ be the position vector of point P_1. It can be represented as

$$_0^0\bar{r}_{P_1} = {}_0^0\bar{r}_{C_1} + {}_{C_1}^0\bar{r}_{P_1} = {}_0^0\bar{r}_{C_1} + {}_1^0R\,{}_{C_1}^1\bar{r}_{P_1}, \tag{1}$$

where $_0^0\bar{r}_{C_1}$ is the position vector of the center of mass of link 1. $_1^0R$ is the orthonormal rotation matrix. The velocity of point P_1 can be obtained by dif-
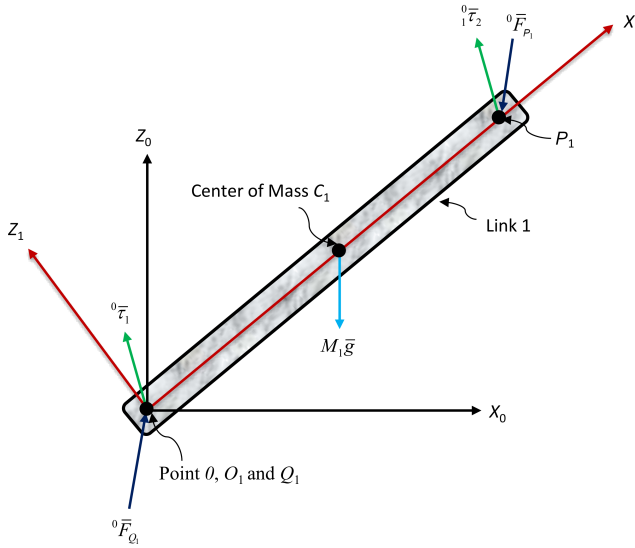
FIG. 3. Link 1 of the spatial mechanism.

ferentiating Eq. (1). Using notation $\frac{d}{dt}x = \dot{x}$ for differentiation with respect to time t, we obtain

$$\begin{smallmatrix}0\\0\end{smallmatrix}\dot{\bar{r}}_{P_1} = \begin{smallmatrix}0\\0\end{smallmatrix}\dot{\bar{r}}_{C_1} - \left[\begin{smallmatrix}0\\C_1\end{smallmatrix}\bar{r}_{P_1}\times \right] \begin{smallmatrix}0\\0\end{smallmatrix}\bar{\omega}_1. \tag{2}$$

Similarly for point Q_1:

$$\begin{smallmatrix}0\\0\end{smallmatrix}\dot{\bar{r}}_{Q_1} = \begin{smallmatrix}0\\0\end{smallmatrix}\dot{\bar{r}}_{C_1} - \left[\begin{smallmatrix}0\\C_1\end{smallmatrix}\bar{r}_{Q_1}\times \right] \begin{smallmatrix}0\\0\end{smallmatrix}\bar{\omega}_1. \tag{3}$$

The kinematic relationship of (2) and (3) can be expressed in the form of a multibond graph, as shown in Fig. 4. Scalar or single bonds are repre-
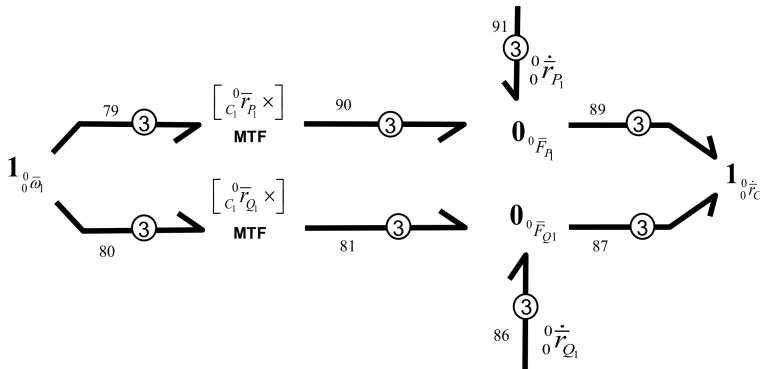
FIG. 4. Sub bond graph for the kinematic relationship of (2) and (3).

sented by the thin harpoon arrows, while the thick harpoon arrows show a multibond with cardinality 3, indicating the number of scalar bonds in a multibond.

When the mass of the link is taken into account, translational and rotational dynamics come into the picture. This is presented in the bond graph of Fig. 5. Let M_1 be the mass of link 1 and $\overline{g}$ be the gravitational acceleration. The translational part of the dynamics is represented by the right side of the bond graph, while the rotational part is shown on the left side.
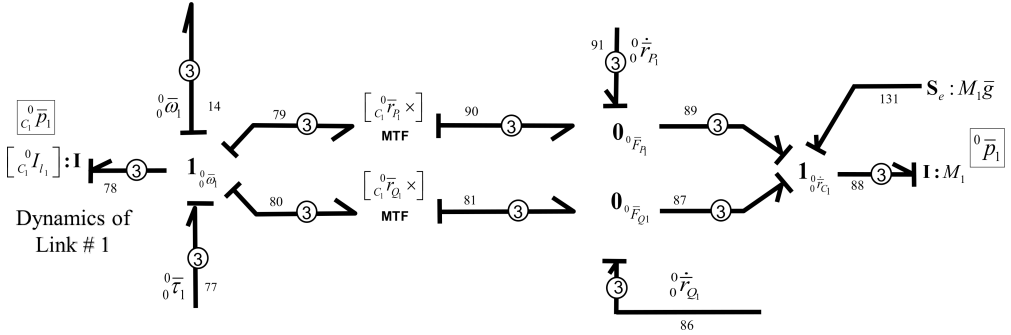
FIG. 5. Bond graph for the dynamics of link 1.

In the bond graph shown in Fig. 5, the inertia element $\mathbf{I} : [m]$ relating to translational dynamics is connected to the common flow junction $1_{0\dot{\overline{r}}_{C_1}}$, while the inertia element $\mathbf{I} : [{}^0_C I_1]$ pertaining to rotational dynamics is connected to the common flow junction $1_{0\overline{\omega}_1}$. ${}^0_0\dot{\overline{r}}_{C_1}$ and ${}^0_0\overline{\omega}_1$ represent the translational velocity and the angular velocity of the link, respectively. By using the same procedure, the bond graph model of each rigid link is prepared and assembled. The systematic procedure to assemble the sub bond graphs of individual links to obtain a complete bond graph of the entire system, has been well explained by Vaz [26] and Mishra and Vaz [28].

During assembling the sub bond graphs of individual links, the derivative causality occurs. The bond graph is converted to an integrally caused type by adding viscoelastic subsystems. The viscoelastic subsystem is modeled using $\boldsymbol{C}$ and $\boldsymbol{R}$ elements. These viscoelastic subsystems act like translational and rotational couplings. Viscoelastic translational and rotational coupling elements are used to join the bond graphs of two links. The use of these couplings makes the model more realistic. A source of flow sf is applied at point P_3 of the mechanism, shown by bond 42 in Fig. 6. The comprehensive multibond graph of the spatial mechanism is presented in Fig. 6.
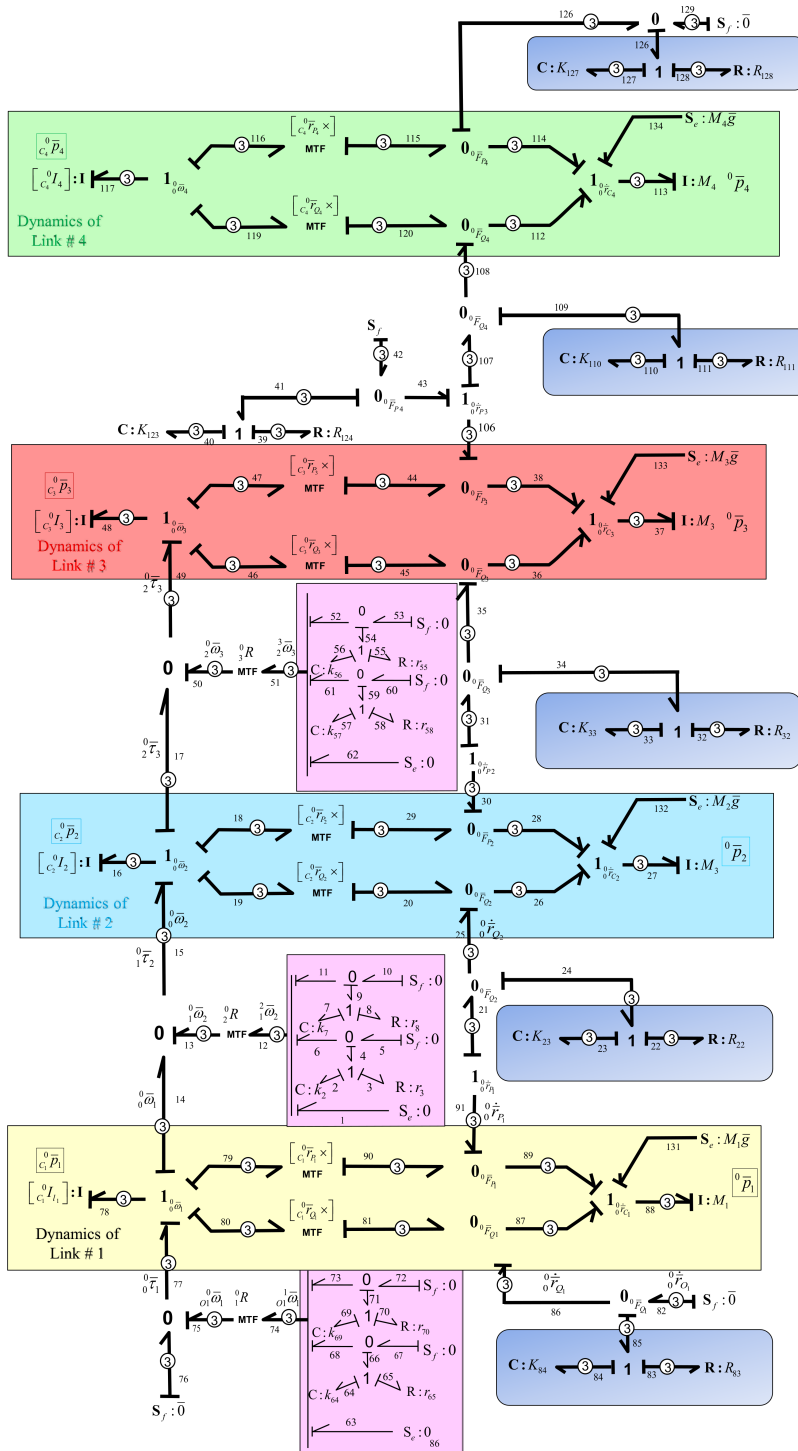
FIG. 6. Complete multibond graph of the spatial mechanism.

3. Various applications of the mechanism

The 3R2S mechanism consists of two spherical joints, one at point P_3 and another at point P_4. These two spherical joints provide the ability for the mechanism to move in 3D space, and the mechanism may be used in various applications. For example, such a mechanism can be used to operate a joystick. It may also be used to operate a gear lever of an automobile. These two applications are modeled using a bond graph and simulated using MATLAB [29]. In the first case, various desired trajectories are provided as input flow to the spherical joint at point P_3. Due to the fixed length of link 4, the actual output trajectory profile at point P_3 is on an imaginary sphere. After the simulation, the results from various plots are analyzed. In the second case, the application in the gear mechanism is discussed.

4. Simulation results and discussion

Initially, the system is considered to be at rest. Each rigid link is considered as a cylindrical rod having a diameter equal to 0.02 m. A flow S_f is given at point P_3 shown by bond 42 in the main bond graph. The bond graph model of the mechanism is simulated and various results are drawn, analyzed and discussed. The simulation code is written in MATLAB [29]. Link properties for the simulation are shown in Table 1. Table 2 shows the values of stiffness and damping elements of various couplings used during the construction of the main bond graph of the entire system.

TABLE 1. Link properties used for simulation.

Length of links [m]			
$l_1 = 0.07$	$l_2 = 0.06$	$l_3 = 0.05$	$l_4 = 0.05$
Mass of links [kg]			
$m_1 = 0.7$	$m_2 = 0.6$	$m_3 = 0.5$	$m_4 = 0.4$
Initial relative angles of links [rad]			
$\theta_1 = 0$	$\theta_2 = \pi/6$	$\theta_3 = -\pi/2$	$\theta_4 = -\pi/6$

4.1. Case 1: Application in operating a joystick

A joystick is a principal controlling device to control civilian and military aircraft. The joystick is like a stick that pivots on a base and reports variations in its angle and direction to the device it is controlling. The 3R2S spatial mechanism may also be used to operate a joystick. In 3R2S mechanism, during the simulation, various trajectories are given as input flow to point P_3. These two desired trajectories and actual trajectories are shown by the various plots. Due

TABLE 2. Stiffness and damping of various couplings for simulation.

Location	Stiffness	Damping
Translational coupling between		
Fixed frame and link 1	$k_{1t} = 10^8$ N/m	$r_{1t} = 50$ N$\cdot$s/m
Link 1 and link 2	$k_{2t} = 10^8$ N/m	$r_{2t} = 50$ N$\cdot$s/m
Link 2 and link 3	$k_{3t} = 10^8$ N/m	$r_{3t} = 50$ N$\cdot$s/m
Link 3 and link 4	$k_{4t} = 10^8$ N/m	$r_{4t} = 50$ N$\cdot$s/m
Link 4 and fixed frame	$k_{5t} = 10^8$ N/m	$r_{5t} = 5$ N$\cdot$s/m
At point p_3 where flow is applied	$k_{ft} = 10^5$ N/m	$r_{ft} = 5$ N$\cdot$s/m
Rotational coupling between		
Fixed frame and link 1	$k_{1rx} = 100$ N$\cdot$m/rad $k_{1ry} = 100$ N$\cdot$m/rad	$R_{1rx} = 1$ N$\cdot$m$\cdot$s/rad $R_{1ry} = 1$ N$\cdot$m$\cdot$s/rad
Link 1 and link 2	$k_{2rx} = 100$ N$\cdot$m/rad $k_{2ry} = 100$ N$\cdot$m/rad	$R_{2rx} = 1$ N$\cdot$m$\cdot$s/rad $R_{2ry} = 1$ N$\cdot$m$\cdot$s/rad
Link 2 and link 3	$k_{3rx} = 100$ N$\cdot$m/rad $k_{3ry} = 100$ N$\cdot$m/rad	$R_{3rx} = 1$ N$\cdot$m$\cdot$s/rad $R_{3ry} = 1$ N$\cdot$m$\cdot$s/rad

to the constrained length of link 4, both the actual trajectory and projected desired trajectory are not coinciding.

In the first case, a circular motion is applied to point P_3. In Fig. 7, point p_3 is shifted outward, covering a distance equal to the radius of the circle. Then a circular motion is provided as input. Actual and desired trajectories are shown in Fig. 7. The orientation of matrix ^0_4R is presented in Fig. 8. The loci covered by unit vectors $^0\widehat{i}_4$, $^0\widehat{j}_4$, and $^0\widehat{k}_4$ are shown in Fig. 8. The loci of unit vectors $^0\widehat{j}_4$ and $^0\widehat{k}_4$ show that link 4 rotates about its own axis. This is due to the

Position of Tip P_3 of Link 3, $^0_0\bar{r}_{P_3}$
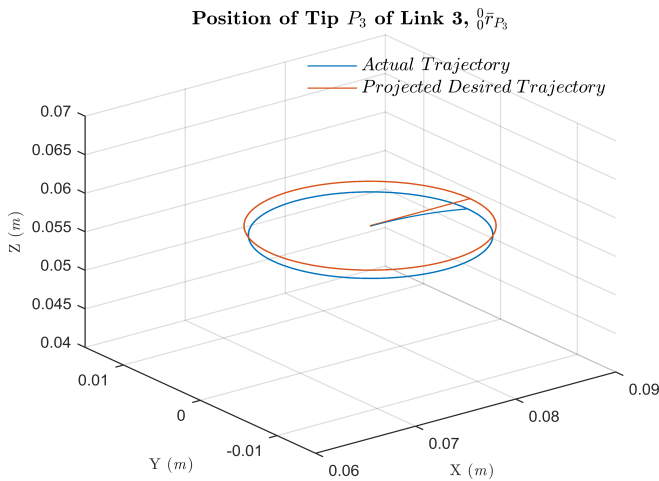
FIG. 7. Projected desired trajectory and actual trajectory of a circular profile.
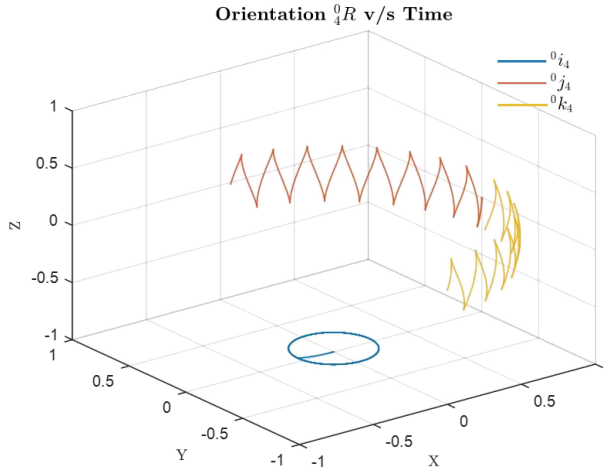
FIG. 8. Orientation of unit vectors of ^0_4R.

gyroscopic effect. $^1_0\theta_1$ is the angle between the X-axis of frame {0} and the X-axis of frame {1}. Similarly, $^2_1\theta_2$ between link 1 and link 2, $^3_2\theta_3$ between link 2 and link 3, and $^4_3\theta_4$ between link 3 and link 4, are relative angles. The variation in relative joint angles $^1_0\theta_1$, $^2_1\theta_2$, $^3_2\theta_3$, and $^4_3\theta_4$ with regard to time is shown in Fig. 9. Initially, point p_3 moves in a straight line to cover a distance equal to the radius, and then the circular motion starts. Figure 9 shows the variation in angle $^1_0\theta_1$, the initial graph is a straight line for 2 seconds, and then the variation in the angle starts.
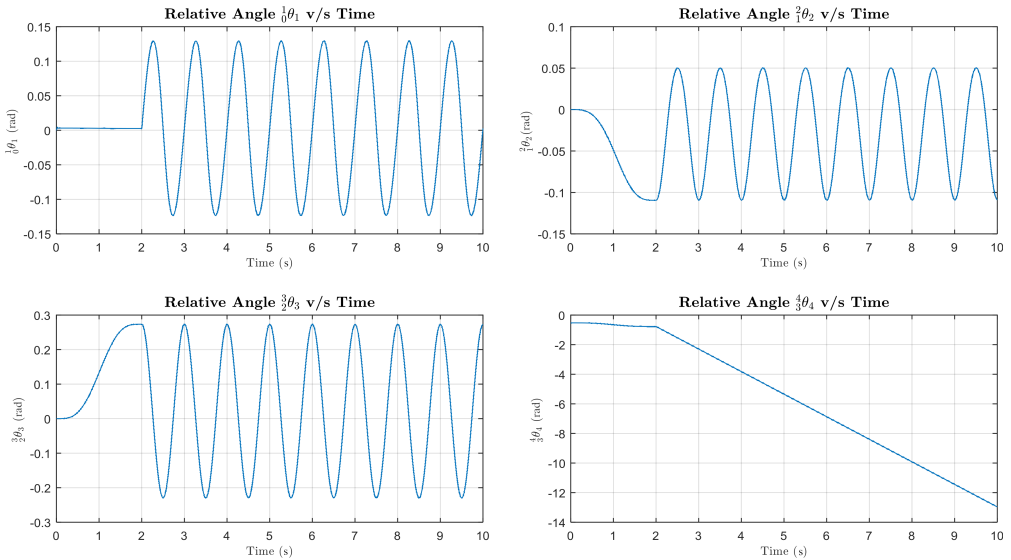
FIG. 9. Variation in joint angles $^1_0\theta_1$, $^2_1\theta_2$, $^3_2\theta_3$, and $^4_3\theta_4$ in time in the case of circular profile.

To control the movement and directions, sometimes different types of movements are applied to the joystick. During the simulation, a path trajectory, shown by the projected desired trajectory in Fig. 10, is applied by the mechanism.

Position of Tip P_3 of Link 3, $_0^0\bar{r}_{P_3}$
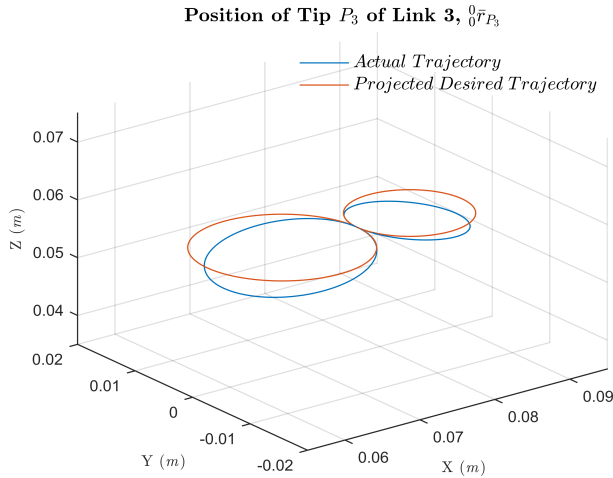
FIG. 10. Projected desired trajectory and actual trajectory.

The actual trajectory given by the system is also shown in Fig. 10. The upper circle shown in the shape of the profile "8" is small compared to the lower circle. The history of relative change in the various joint angles versus time is shown in Fig. 11. The graph of the variation in relative angle $_0^1\theta_1$ shows that the total time
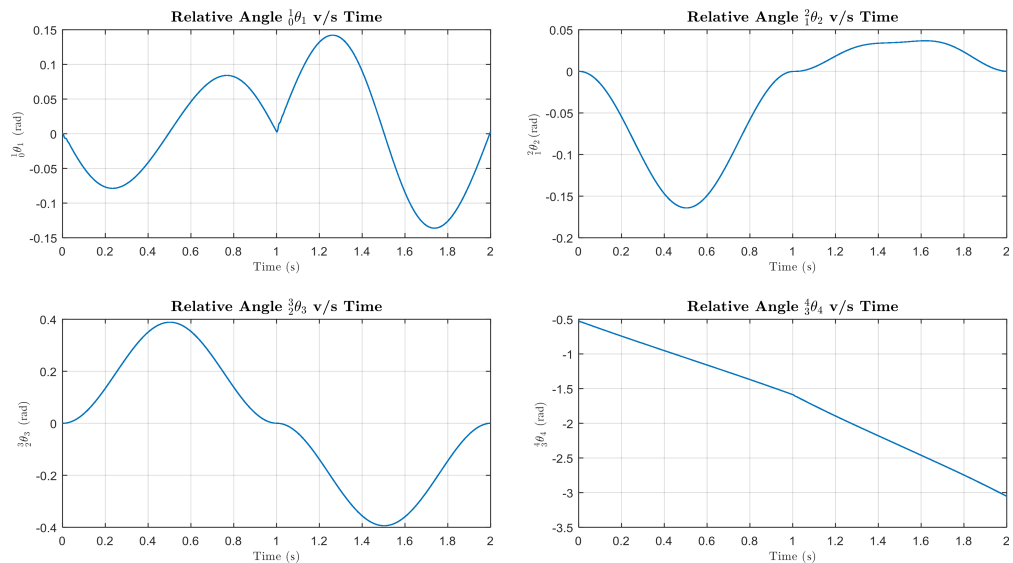
FIG. 11. Variation in joint angles $_0^1\theta_1$, $_1^2\theta_2$, $_2^3\theta_3$, and $_3^4\theta_4$ in time.

taken by point P_3 is 2 seconds. The variation in angle takes place from -0.07 radians to 0.07 radians for the first circle and from -1.14 radians to 1.14 radians for the other circle. Similarly, variations in other angles are shown in Fig. 11.

4.2. Case 2: Application in operating a lever of a gear mechanism

Another important application of the 3R2S spatial mechanism is in operating a gear lever in an automobile. To shift the gear lever, various movements to the lever are applied. An example, showing the application of the 3R2S mechanism in operating automobile gear, is shown in Fig. 12. The input movement applied to the gear lever is shown by the desired projected trajectory in red color, while the actual trajectory is shown using a blue line.
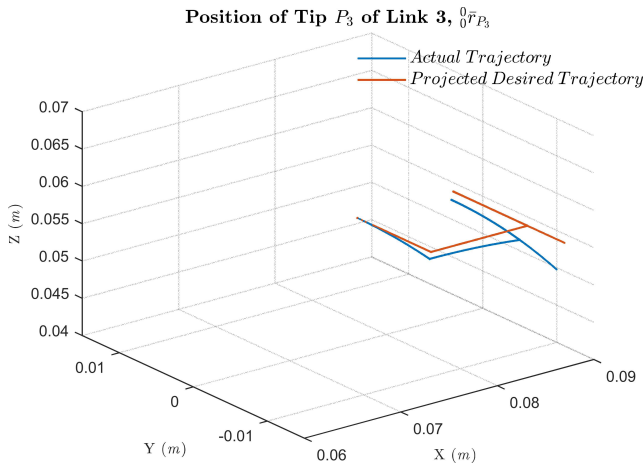
FIG. 12. Projected desired trajectory and actual trajectory of the profile used in the gear mechanism.

The changes in the relative joint angles versus time are presented in Fig. 13. The plot shows that the total time taken by point P_3, to complete the desired trajectory is 10 seconds. The angle covered by each link in radians is shown in Fig. 13. The angle changes within the range of 0.04 radians to -0.17 radians. The angle may be computed at any position from the plot. The changes in other relative angles are also observed in Fig. 13.

5. CONCLUSION

In summary, the methodology for inverse kinematics using the bond graph approach has been explained and demonstrated using the example of a 3R2S spatial mechanism. The uses of such a mechanism were studied for operating
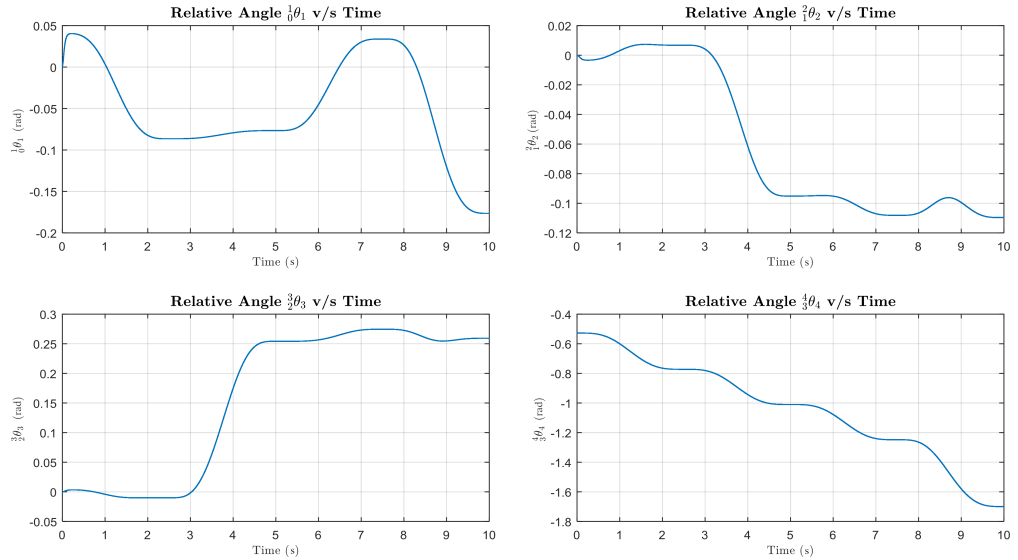
FIG. 13. Variation in joint angles $_0^1\theta_1$, $_1^2\theta_2$, $_2^3\theta_3$, and $_3^4\theta_4$ in time in the profile used in the gear mechanism.

a joystick and operating the gear lever of an automobile. In these applications, the joint angle trajectories required to obtain the desired motion of the end effector were obtained using the above methodology for inverse kinematics from the bond graph model. The simulation code has been generated algorithmically, directly from the bond graph.

The ideas developed in this paper can be employed to determine and control joint forces and joint torques at various joints for various mechanisms used in a wide range of applications.

Acknowledgments

References

1. R.M. Murray, Z. Li, S.S. Sastry, *A mathematical introduction to robotic manipulation*, CRC Press, 1994, doi: 10.1.1.169.3957.

2. A. Ghosh, A.K. Mallik, *Theory of mechanisms and machines*, East-West Press (P) Ltd., New Delhi, 2006.

3. J.J. Craig, *Solutions Manual. Introduction to robotics: mechanics and control*, Pearson Education Inc., 2005.

4. K.J. Waldron, G.L. Kinzel, *Kinematics, dynamics and design of machinery*, 2nd ed., Wiley & Sons, 2004.

5. J.J. Dicker Jr., G.R. Pennock, J.E. Shigley, *Theory of machine and mechanisms*, 3rd ed., Oxford University Press, New Delhi, 2009.

6. H. Goldstein, *Classical mechanics*, Narosa Publishing House, 1995.

7. F.T. Brown, Bond graphs for nonholonomic dynamic systems, *Journal of Dynamic Systems, Measurement, and Control*, **98**(4): 361–366, 1976, doi: 10.1115/1.3427052.

8. M.J.L. Tiernego, A.M. Bos, Modelling the dynamics and kinematics of mechanical systems with multibond graphs, *Journal of the Franklin Institute*, **319**(1–2): 37–50, 1985, doi: 10.1016/0016-0032(85)90063-8.

9. E.P. Fahrenthold, J.D. Wargo, Vector and tensor based bond graph for physical systems modeling, *Journal of the Franklin Institute*, **328**(5/6): 833–853, 1991.

10. D.C. Karnopp, Understanding multibody dynamics using bond graph representations, *Journal of the Franklin Institute*, **334**(4): 631–642, 1997, doi: 10.1016/S0016-0032(96)00083-X.

11. A. Mukherjee, R. Karmarkar, *Modelling and simulation of engineering systems through bond graphs*, Narosa Publishing House, New Delhi, 2000.

12. D.C. Karnopp, D.L. Margolis, R.C. Rosenberg, *System dynamics: modeling and simulation of mechatronic systems*, Wiley-InterScience, New York, 2000.

13. D.C. Karnopp, Power-conserving transformations: physical interpretations and applications using bond graphs, *Journal of the Franklin Institute*, **288**(3): 175–201, 1969, doi: 10.1016/0016-0032(69)00246-8.

14. A.M. Bos, M.J.L. Tiernego, Formula manipulation in the bond graph modelling and simulation of large mechanical systems, *Journal of The Franklin Institute*, **319**(1–2): 51–65, 1985, doi: 10.1016/0016-0032(85)90064-X.

15. A. Zeid, C.-H. Chung, Bond graph modeling of multibody, systems: a library, of three-dimensional joints, *Journal of The Franklin Institute*, **319**(4): 605–636, 1992, doi: 10.1016/0016-0032(92)90076-S.

16. J. Jang, C. Han, Proposition of a modeling method for constrained mechanical systems based on the vector bond graph, *Journal of the Franklin Institute*, **335**(3): 451–469, 1998, doi: 10.1016/S0016-0032(96)00129-9.

17. G. Dauphin-Tanguy, A. Rahmani, C. Sueur, Bond graph aided design of controlled systems, *Simulation Practice and Theory*, **7**(5): 493–513, 1999, doi: 10.1016/S0928-4869(99)00009-9.

18. A. Vaz, S. Hirai, Modeling a hand prosthesis with word bond graph objects, *Systems, Man and Cybernetics*, **5**: 4508–4513, 2003, doi: 10.1109/ICSMC.2003.1245694.

19. A. Vaz, P. Sharma, R. Atri, Modeling and simulation of the dynamics of crankshaft-connecting rod-piston-cylinder mechanism and a universal joint using the bond graph approach, *14th National Conference on Machines and Mechanisms (NaCoMM09)*, NIT, Durgapur, India, Dec. 17–18, pp. 298–303, 2009, http://www.nacomm09.ammindia.org/NaCoMM-2009/nacomm09_final_pap/DVAM/DVAMAV3.pdf.

20. A. Vaz, G.K. Thommen, Modeling and simulation of the dynamics of the quick return mechanism: a bond graph approach, *10th National Conference on Industrial Problems on Machines and Mechanisms (IPRoMM 2010)*, MNIT, Jaipur, Dec. 17–18, (IPRoMM), pp. 23–30, 2010.

21. W. Favre-Marquis, S. Scavarda, Alternative causality assignment procedures in bond graph for mechanical systems, *Journal of Dynamic Systems, Measurement, and Control*, **124**(3): 457–463, 2002, doi: 10.1115/1.1481369.

22. F.T. Brown, Lagrangian bond graphs, *Journal of Dynamic Systems, Measurement, and Control*, **94**(3): 213–221, 1972, https://doi.org/10.1115/1.3426591.

23. D. Karnopp, Lagrange's equations for complex bond graph systems, *Journal of Dynamic Systems, Measurement, and Control*, **99**(4): 300–306, 1977, doi: 10.1115/1.3427123.

24. D. Karnopp, Alternative bond graph causal patterns and equation formulations for dynamic systems, *Journal of Dynamic Systems, Measurement, and Control*, **105**(59): 58–63, 1983, doi: 10.1115/1.3149645.

25. F.T. Brown, Hamiltonian and Lagrangian bond graphs, *Journal of the Franklin Institute*, **328**(5–6): 809–831, 1991, doi: 10.1016/0016-0032(91)90056-9.

26. A. Vaz, *Bond graph modeling for rigid body dynamics*, Lecture Notes, 2008.

27. N. Mishra, A. Vaz, Bond graph modeling of a 3-joint string-tube actuated finger prosthesis, *Mechanism and Machine Theory*, **117**: 1–20, 2017, doi: 10.1016/j.mechmachtheory.2017.06.018.

28. N. Mishra, A. Vaz, Modeling and simulation of dynamics of a three dimensional teeter toy using bond graph, *Proceedings of the 1st International Conference on Artificial Intelligence, Modelling and Simulation*, *AIMS*, Kota Kinabalu, Malaysia, Dec. 3–5, 2013, pp. 227–232, 2014, doi: 10.1109/AIMS.2013.43.

29. MATLAB 7.9.0 The MathWorks, Inc., R2016a.